Wind Sensing and Estimation Using Small Fixed-Wing UAVs: A Survey

Pengzhi Tian* and Haiyang Chao†
University of Kansas, Lawrence, KS, 66045

Matthew Rhudy‡
Pennsylvania State University, Reading, PA, 19610

Jason Gross§
West Virginia University, Morgantown, WV, 26506

Huixuan Wu¶
University of Kansas, Lawrence, KS, 66045

I. Introduction

Wind and turbulence have a significant impact on unmanned aerial vehicle (UAV) flight safety and efficiency, especially for challenging missions such as Urban Air Mobility (UAM) flights and beyond visual line of sight (BVLOS) operations. Accurate wind measurement/estimation can provide important information regarding the uncertain environment of aircraft during flight (e.g., extreme winds during wildfire, wake vortex in close formation flight, or strong turbulence in urban cities). Knowledge of the current local wind field is beneficial to feedback control algorithms in maintaining safe and robust flight in an uncertain environment. In addition, efficiency of flight can also be improved, for example, through trajectory planning and optimization based on the local wind patterns (e.g., thermal soaring). However, it is not easy to measure or estimate winds surrounding aircraft despite their persistent existence. The challenges come from the cost and payload limit of small UAVs as well as strong spatio-temporal variations of wind fields. The general problem of wind sensing and estimation using small UAVs can be divided into two sub-problems, (1) wind sensing and estimation along the UAV flight trajectory at specific time and locations; (2) wind field estimation by considering the spatio-temporal characteristics of wind.

The classical wind sensing and estimation problem along the aircraft flight trajectory can be tackled by solving the wind triangulation, which is illustrated in Fig. 1, where $\boldsymbol{V_g}$ is the ground speed, $\boldsymbol{V}$ is the airspeed, $\boldsymbol{V_w}$ is the wind speed, α is the angle of attack, and β is the sideslip angle [1, 2]. The wind triangle equation expressed in the north-east-down

*Ph.D. Student, Aerospace Engineering Department, University of Kansas, Lawrence, KS, 66045. E-mail: pengzhitian@ku.edu.
†Associate Professor, Aerospace Engineering Department, University of Kansas, Lawrence, KS, 66045. E-mail: chaohaiyang@ku.edu.
‡Assistant Professor, Division of Engineering, Business, and Computing, Pennsylvania State University, Reading, PA, 19610. E-mail: mbr5002@psu.edu
§Associate Professor, Department of Mechanical and Aerospace Engineering, West Virginia University, Morgantown, WV, 26506. E-mail: jason.gross@mail.wvu.edu.
¶Assistant Professor, Aerospace Engineering Department, University of Kansas, Lawrence, KS, 66045. E-mail: hwu@ku.edu.

(NED) earth-fixed local frame is shown in Eq. (1)

$$\begin{bmatrix} \mathrm{w}_n \\ \mathrm{w}_e \\ \mathrm{w}_d \end{bmatrix} = \begin{bmatrix} V_n \\ V_e \\ V_d \end{bmatrix} - \boldsymbol{R}_{\boldsymbol{b}}^{\boldsymbol{n}}(\phi, \theta, \psi) \begin{bmatrix} u \\ v \\ w \end{bmatrix}, \tag{1}$$

where $[V_n, V_e, V_d]$ is the ground velocity expressed in the NED frame, $[u, v, w]$ is the airspeed expressed in the body frame, $[\mathrm{w}_n, \mathrm{w}_e, \mathrm{w}_d]$ is the wind speed expressed in the NED frame, and $\boldsymbol{R}_{\boldsymbol{b}}^{\boldsymbol{n}}(\phi, \theta, \psi)$ is the rotation matrix from the body frame to the NED frame shown in Eq. (2)

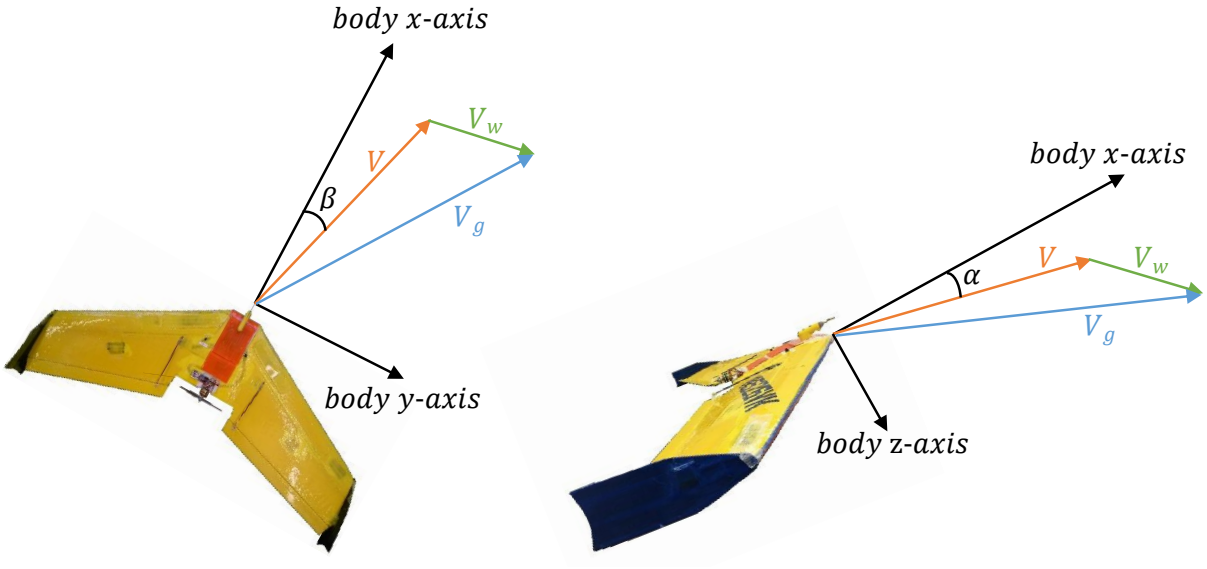

Fig. 1 Wind triangle illustration.

$$\boldsymbol{R}_{\boldsymbol{b}}^{\boldsymbol{n}}(\phi, \theta, \psi) = \begin{bmatrix} \cos\psi\cos\theta & -\sin\psi\cos\phi + \cos\psi\sin\theta\sin\phi & \sin\psi\sin\phi + \cos\psi\sin\theta\cos\phi \\ \sin\psi\cos\theta & \cos\psi\cos\phi + \sin\psi\sin\theta\sin\phi & -\cos\psi\sin\phi + \sin\psi\sin\theta\cos\phi \\ -\sin\theta & \cos\theta\sin\phi & \cos\theta\cos\phi \end{bmatrix}. \tag{2}$$

Given Eq. (1), the most straight forward way for UAV-based wind sensing is to directly measure all the related states in the equation and perform direct calculations. However, not every wind-related state can be easily or accurately measured for small UAVs. For example, only a small percentage of UAVs is equipped with an air data system (ADS) to measure air triplets, including the airspeed V, angle of attack AOA/α, and sideslip angle AOS/β. With measured

$[V, \alpha, \beta]$, $[u, v, w]$ can be calculated using Eq. (3)

$$\begin{bmatrix} u \\ v \\ w \end{bmatrix} = V \begin{bmatrix} \cos\alpha \cos\beta \\ \sin\beta \\ \sin\alpha \cos\beta \end{bmatrix}. \tag{3}$$

Additionally, an ADS that can provide accurate air triplet measurements is usually very expensive and requires extensive calibration. Meanwhile, UAVs, especially small ones, are usually limited by space and weight. In recent years, the development of cheaper, smaller, and more powerful microprocessors and sensors makes it possible to use delicately designed stochastic algorithms to solve these problems. Ultimately, it becomes a trade-off between direct measurements (hardware/sensors) and estimation (software/algorithms).

Given measured or estimated wind information along the UAV trajectory, the spatio-temporal variations of the wind field can be further derived. This requires accurate wind measurements or estimates at specific time and locations, as well as appropriate models for accurate wind field interpolation, extrapolation, or reconstruction. The simplest approach is to assume that the wind field is frozen, or the wind field does not change in a relatively short time period. Spatial variations of the wind field can then be treated as functions of 3D positions. For certain applications like thermal soaring, the problem can be further simplified by considering wind variations in only one dimension, usually in the vertical direction. Alternatively, wind field can be analyzed from perspectives of power spectral density (PSD) or total energy with the focus on the wind energy distribution and its impact on UAVs instead of spatio-temporal variations.

In the last decade, both fixed-wing UAVs and rotary-wing UAVs have been increasingly used for wind sensing and estimation problem. These two types of UAV platforms are actually complementary to each other. Fixed-wing UAVs are more used for long range missions and gust and turbulence sensing [3]. And rotary-wing UAVs (e.g. quadcopters) work better for vertical wind profile estimation, given their hovering capability [4, 5].

This paper provides a comprehensive survey of existing wind sensing and estimation methods using small fixed-wing UAVs, including wind models, sensors, UAV-wind interaction modeling, and estimation algorithms. The objective is to provide an overview of the state of the art UAV-based wind estimation methods in a hope to motivate new breakthroughs in the interdisciplinary area of guidance, navigation, and control (GNC) and aerodynamic or fluid dynamic communities. This paper can also serve as a selection guide for researchers who want to develop customized UAVs for wind measurements. The major contributions of this paper can be summarized as follows:

1) A survey of typical wind models for UAV-based wind sensing and estimation;
2) A survey of available sensors for UAV-based wind sensing and estimation;
3) A summary of existing solutions for UAV-based wind sensing and estimation;
4) Recommendations for wind model, sensor, and algorithm selection and potential future directions for UAV-based

wind estimation.

The organization of this paper can be summarized as follows. The wind representation and modeling are described in Sec. II. Available UAV sensors for wind sensing and estimation are introduced and compared in Sec. III. Sec. IV explains the UAV-wind interaction modeling. Summaries of existing work and recommendations for selection of wind models, sensors, and algorithms are presented in Sec. V, together with potential future directions. Conclusions are made in Sec. VI.

II. Wind Representation for State Estimation Purpose

The wind can be generally described as the superposition of mean wind, discrete gust, and turbulence [6–8]. Mean wind speed is the wind speed averaged over a specific time interval, which can also be treated as the prevailing wind for many cases. In contrast, a gust is a brief and sudden increase in wind speed along a specific direction, the duration of which is usually less than 20 seconds. Turbulence is an irregular motion of the air resulting from eddies and vertical currents [9]. In this paper, different types of wind representations are surveyed for the wind estimation problem including time domain representation, frequency domain representation, spatial description, and CFD models. Most of the provided wind models have been used in wind estimation filter design.Note that equations shown in this section are specifically chosen such that they can be easily or have a great potential to be incorporated into estimation filters.

A. Time Domain Wind Representation

Due to the non-deterministic nature of wind, stochastic models such as the Gauss-Markov (GM) model has been used to represent wind speed changes [10, 11]. A general GM model is given in discrete time by

$$\boldsymbol{\mu}_k = e^{-T_s/\tau}\boldsymbol{\mu}_{k-1} + \mathbf{w}_k^{GM}, \tag{4}$$

where $\boldsymbol{\mu}_k$ is the system state at the current time stamp, $\boldsymbol{\mu}_{k-1}$ is the system state at the previous time stamp, T_s is the sampling time, τ is the correlation time of the GM process, and $\mathbf{w}_k^{GM}$ is the driven noise [11]. Especially, the random walk (RW) model, a special case of the GM model that assumes infinite correlation time, is the most popular model within Kalman filtering applications since it matches the discrete-time recursive stochastic framework nicely and has little difference in performance compared with the general GM model as shown in previous work [11, 12]. Two of the most commonly used temporal wind models are the first order and the second order RW models, which are based on Gaussian RW processes and Markov chain models. Although these two temporal models do not consider the long-time correlation in a turbulent wind field, they are widely used in the wind energy community for synthetic wind speed generations and prevailing wind estimation for their simplicity [13, 14].

1. First Order Random Walk Model

By assuming wind dynamics as first order Gaussian RW processes, the wind model can be derived as Eq. (5)

$$\begin{bmatrix} \dot{\mathrm{w}}_n \\ \dot{\mathrm{w}}_e \\ \dot{\mathrm{w}}_d \end{bmatrix} = \begin{bmatrix} \mu_n \\ \mu_e \\ \mu_d \end{bmatrix} = \begin{bmatrix} 0 \\ 0 \\ 0 \end{bmatrix} + \mathbf{w_{wk}}, \tag{5}$$

where $\mathbf{w_{wk}}$ is zero-mean white Gaussian noise vector and $[\mu_n, \mu_e, \mu_d]$ is the wind acceleration expressed in the NED frame.

2. Second Order Random Walk Model

Similarly, wind dynamics can be modeled as second order Gaussian RW processes as shown in Eq. (6) and Eq. (7)

$$\begin{bmatrix} \dot{\mathrm{w}}_n \\ \dot{\mathrm{w}}_e \\ \dot{\mathrm{w}}_d \end{bmatrix} = \begin{bmatrix} \mu_n \\ \mu_e \\ \mu_d \end{bmatrix}, \tag{6}$$

$$\begin{bmatrix} \ddot{\mathrm{w}}_n \\ \ddot{\mathrm{w}}_e \\ \ddot{\mathrm{w}}_d \end{bmatrix} = \begin{bmatrix} \dot{\mu}_n \\ \dot{\mu}_e \\ \dot{\mu}_d \end{bmatrix} = \begin{bmatrix} 0 \\ 0 \\ 0 \end{bmatrix} + \mathbf{w_{\mu k}}, \tag{7}$$

where $\mathbf{w_{\mu k}}$ is a zero-mean white Gaussian noise vector.

Compared with the first order RW process, the second order RW process has a longer memory of historical data and the underlying correlation. Researchers have found that the second order RW process is more accurate in generating synthetic wind speed time series [13, 14]. Another advantage of using the second order RW model is that it allows wind accelerations be explicitly included in the UAV dynamic equations, as shown in Eq. (8) [1]

$$\begin{bmatrix} \dot{u} \\ \dot{v} \\ \dot{w} \end{bmatrix} = \begin{bmatrix} -qw + rv - g\sin\theta + a_x \\ -ru + pw + g\cos\theta\sin\phi + a_y \\ -pv + qu + g\cos\theta\cos\phi + a_z \end{bmatrix} - \boldsymbol{R_n^b}(\phi, \theta, \psi) \begin{bmatrix} \mu_n \\ \mu_e \\ \mu_d \end{bmatrix}, \tag{8}$$

where $[p, q, r]$ are rotation rates and $\boldsymbol{R_n^b}(\phi, \theta, \psi) = \boldsymbol{R_b^n}(\phi, \theta, \psi)^\intercal$ is the rotation matrix from the NED frame to the body

frame. However, as more states are introduced in the second order RW model, it becomes more complex and may generate more challenges for the tuning of wind estimation stochastic filters.

B. Frequency Domain Wind Representation

In addition to the time domain wind modeling, frequency domain models, especially PSD models, are also widely used to represent wind variations. Frequency domain models can provide information of wind energy distribution across different frequencies. PSD is often used for turbulence modeling and for flight controller validation. A continuous gust profile is also referred to as turbulence. The turbulence $\boldsymbol{V}_{\mathbf{w}_t}$ can be considered as the combination of a series of individual gust and is often idealized as a stationary Gaussian random process. A stationary Gaussian random process can be generated by the superposition of an infinite number of sinusoidal components using Eq. (9) [15]

$$\mathbf{V}_{\mathrm{w_t}}(t) = \sum_{k=1}^{\infty} \sqrt{\Phi(\omega_k)\Delta\omega}\cos(\omega_k t + \Psi_k), \tag{9}$$

where $\Phi(\omega_k)$ is the PSD function, ω_k is the frequency of each individual component, and Ψ_k is the random phase angle. Among a variety of continuous gust models, the von Kármán and Dryden models are most commonly used PSD functions for flight controller design and turbulence modeling in aircraft gust load analysis.

1. Dryden Wind Turbulence Model

The mathematical expressions for the Dryden wind turbulence model are shown in Eqs. (10) - (15) [16]

$$\Phi_{u_{\mathrm{w}_t}}(\omega) = \frac{2\sigma_u^2 L_u}{\pi V} \cdot \frac{1}{1 + \left(L_u \frac{\omega}{V}\right)^2}, \tag{10}$$

$$\Phi_{v_{\mathrm{w}_t}}(\omega) = \frac{\sigma_v^2 L_v}{\pi V} \cdot \frac{1 + 3\left(L_v \frac{\omega}{V}\right)^2}{\left[1 + \left(L_v \frac{\omega}{V}\right)^2\right]^2}, \tag{11}$$

$$\Phi_{w_{\mathrm{w}_t}}(\omega) = \frac{\sigma_w^2 L_w}{\pi V} \cdot \frac{1 + 3\left(L_w \frac{\omega}{V}\right)^2}{\left[1 + \left(L_w \frac{\omega}{V}\right)^2\right]^2}, \tag{12}$$

$$\Phi_{p_t}(\omega) = \frac{\sigma_w^2}{V L_w} \cdot \frac{0.8\left(\frac{\pi L_w}{4b}\right)^{\frac{1}{3}}}{1 + \left(\frac{4b\omega}{\pi V}\right)^2}, \tag{13}$$

$$\Phi_{q_t}(\omega) = \frac{\pm\left(\frac{\omega}{V}\right)^2}{1 + \left(\frac{4b\omega}{\pi V}\right)^2} \cdot \Phi_{w_{\mathrm{w}_t}}(\omega), \tag{14}$$

$$\Phi_{r_t}(\omega) = \frac{\mp\left(\frac{\omega}{V}\right)^2}{1+\left(\frac{3b\omega}{\pi V}\right)^2} \cdot \Phi_{v_{w_t}}(\omega), \tag{15}$$

where $[\Phi_{u_{w_t}}(\omega), \Phi_{v_{w_t}}(\omega), \Phi_{w_{w_t}}(\omega)]$ represent power spectral densities of turbulence along the UAV's body axes $\boldsymbol{V}_{\mathbf{w_t}}$ $[u_{w_t}, v_{w_t}, w_{w_t}]$. $[\Phi_{p_t}(\omega), \Phi_{q_t}(\omega), \Phi_{r_t}(\omega)]$ represent power spectral densities for three angular velocity components caused by turbulence $[p_t, q_t, r_t]$. b is the aircraft wingspan, σ_* is the turbulence intensity along aircraft boy axis, and L_* is the turbulence length scale along aircraft boy axis, which is a function of altitude. Note that $_t$ stands for turbulence.

2. Von Kármán Wind Turbulence Model

The von Kármán wind turbulence model describes the continuous gusts by using similar parameters as the Dryden wind turbulence model. The major difference between these two models is that the von Kármán model has irrational PSDs for linear velocity components while the Dryden model has rational ones. Mathematical expressions for the von Kármán model are shown in Eq. (16) - (18) [17]

$$\Phi_{u_{w_t}}(\omega) = \frac{2\sigma_u^2 L_u}{\pi V} \cdot \frac{1}{\left[1+\left(1.339 L_u \frac{\omega}{V}\right)^2\right]^{\frac{5}{6}}}, \tag{16}$$

$$\Phi_{v_{w_t}}(\omega) = \frac{\sigma_v^2 L_v}{\pi V} \cdot \frac{1+\frac{8}{3}\left(1.339 L_v \frac{\omega}{V}\right)^2}{\left[1+\left(1.339 L_v \frac{\omega}{V}\right)^2\right]^{\frac{11}{6}}}, \tag{17}$$

$$\Phi_{w_{w_t}}(\omega) = \frac{\sigma_w^2 L_w}{\pi V} \cdot \frac{1+\frac{8}{3}\left(1.339 L_w \frac{\omega}{V}\right)^2}{\left[1+\left(1.339 L_w \frac{\omega}{V}\right)^2\right]^{\frac{11}{6}}}, \tag{18}$$

whereas power spectral densities for three angular velocity components of von Kármán turbulence are the same with those in the Dryden turbulence model, shown in Eq. (13) - (15).

Note that, both models assume the wind turbulence is varying in space but frozen in time, and they rely on the UAV's motion through the turbulence field to generate temporal variations in wind speed (they are expressed in the UAV's body frame instead of the NED frame). These two turbulence models can be incorporated into the UAV's equations of motion as wind disturbances [18]. Compared with the Dryden model, the von Kármán model generally fits the wind measurements better. However, the desired filter implementations of the von Kármán model can only be approximated due to its irrational PSDs. Both models can be simulated using MATLAB, with the details provided in [1, 19, 20].

C. Spatial Wind Description

In addition to temporal wind speed correlations, certain wind fields also have strong correlations with the spatial information. Examples include mountain waves, thermal wind, and aircraft wake vortex. A general spatial wind field can be modeled by a function correlating 3D wind speed and 3D positions. The most intuitive way of finding the correlation

function is using a polynomial, which may be difficult to find for a general wind field. Empirical modeling can be used instead to model certain types of spatial wind fields based on former experience and measurements. Example empirical models include wind shear model, discrete gust model, and thermal model [16, 21, 22].

1. Wind Shear Model

There are two wind shear models that are widely used [21]. The first one is the wind profile power law, shown in Eq. (19) [23]

$$V_{\mathrm{w}_h} = V_{\mathrm{w}_{h_r}} \left(\frac{h}{h_r}\right)^{\gamma}, \tag{19}$$

where V_{w_h} is the horizontal wind speed $\sqrt{{\mathrm{w}_n}^2 + {\mathrm{w}_e}^2}$, h is the altitude, and h_r is the altitude that the reference horizontal wind speed $V_{\mathrm{w}_{h_r}}$ is measured. The wind shear exponent γ is an empirical coefficient, which varies with the stability condition of the atmosphere. For nominal conditions, γ is approximately $1/7$. The second one is the wind profile log law, shown in Eq. (20) [24]

$$V_{\mathrm{w}_h} = V_{\mathrm{w}_{h_6}} \frac{\ln\left(\frac{h}{z_0}\right)}{\ln\left(\frac{6}{z_0}\right)}, \tag{20}$$

where $V_{\mathrm{w}_{h_6}}$ is the horizontal wind speed measured at 6 meters above the ground and z_0 is an empirical constant. Both models can be used to predict or extrapolate wind speed at a certain altitude given horizontal wind measurements from other altitudes. The wind shear model is widely used in UAV dynamic soaring researches for flight endurance extension.

2. One-minus-cosine Gust Model

One widely used idealized gust model is the one-minus-cosine gust model. The one-minus-cosine model is often used to describe an individual gust, or so called a discrete gust [16]. The discrete gust model usually assumes the gust velocity to be one dimensional, which is acting normally along the aircraft body x, y, or z axis for longitudinal or lateral motion analysis. The mathematical expression for the one-minus-cosine model is shown in Eq. (21)

$$V_{\mathrm{w}_g} = \begin{cases} 0 & x < 0 \\ \frac{V_{m_g}}{2}\left(1 - \cos\left(\frac{\pi x}{d_{m_g}}\right)\right) & 0 \le x \le d_{m_g} \\ V_{m_g} & x > d_{m_g} \end{cases}, \tag{21}$$

where V_{m_g} is the gust amplitude, d_{m_g} is the gust length, x is the distance traveled, and V_{w_g} is the resultant wind velocity in the body frame. Note that $_g$ stands for the discrete gust.

3. Thermal Model

Thermals, commonly referred to as updrafts, are columns of rising air generated by the uneven ground surface heating. The vertical wind speed within an individual thermal column decays from the maximum magnitude at the thermal center following a bell shape, as shown in Eq. (22) [22]

$$\mathrm{w}_z(x,y) = \mathrm{w}_z(x_0,y_0)e^{-\left(\frac{(x-x_0)^2+(y-y_0)^2}{{R_0}^2}\right)}\left[1-\left(\frac{(x-x_0)^2+(y-y_0)^2}{{R_0}^2}\right)\right], \tag{22}$$

where $\mathrm{w}_z(x,y)$ is the vertical wind speed at position (x,y), (x_0,y_0) is the position of the thermal center/core, and R_0 is the radius of the thermal column. In this model, the thermal column is assumed to be stationary, where its position and vertical speed distribution does not change over the time. The study of thermals can help develop small UAVs with the capabilities to extract energy from the atmosphere (static soaring) for long range flight.

4. Wake Vortex Model

Wake vortex, also known as wake turbulence, is an atmospheric disturbance that generated by a flying aircraft when the air below the wing circulates around the wingtip due to the pressure difference. The generated wingtip vortices are counter-rotating pairs that trail from wingtips and can remain in the air for several minutes after the aircraft flies by Burnham-Hallock model, a commonly used wake vortex model of the tangential velocity field, is shown in Eq. (23) [25, 26]

$$\mathrm{w}_\theta(r) = \frac{\Gamma_0}{2\pi r}\frac{r^2}{r^2+r_c^2}, \tag{23}$$

where Γ_0 is the initial wake vortex strength, r_c is the vortex core radius, r is the radial distance to the vortex filament center line, and $\mathrm{w}_\theta(r)$ is the tangential velocity of wake vortex at distance r from the vortex center. The initial wake vortex strength is primarily determined by the airspeed and the weight (lift) of the aircraft. The decaying of the generated wake vortex can be described as different models such as Sarpkaya decay model [27]. Real time measurement of wake vortex locations is critical to fuel saving formation flight of manned and unmanned aircraft [28].

D. Other Wind Models

Other than the models mentioned before, the wind field can also be obtained using CFD methods, which are able to consider complex terrain and weather conditions [29, 30]. The simulations are usually based on the governing equations of air flow and specific boundary conditions; thus, the results are much closer to those obtained with the above empirical models. In ideal conditions, the CFD can also provide the turbulent field information in addition to prevailing wind. However, CFD models are often computationally expensive, especially for large scales. Currently, it is difficult to resolve the entire flow in a field of 1 km scale. Certain closure models, such as large eddy models, are usually involved. In a smaller scale similar to a UAV, the CFD can be used to accurately estimate lift, drag, and torque. Consequently,

the flight response can be modeled. In the future, the integration of large-scale wind simulation and small-scale flight response estimation will lead to the development of better UAV control algorithms.

III. UAV Sensors for Wind Sensing and Estimation

The impact of wind and turbulence on aircraft can be modeled by aircraft kinematics and dynamics equations [1]. Sensors presented in this section are those commonly used or have the potential to be used on small fixed-wing UAVs to facilitate the sensing and estimation of wind fields. Main consideration factors include their size and weight. Based on Eq. (1) and Eq. (3) and considering wind field estimation requirements, the recommended sensors can be summarized as four major categories.

1) Sensors to measure/estimate the UAV's 3D position $[P_n, P_e, P_d]$ and ground velocity $[V_n, V_e, V_d]$, which are required to solve wind triangulation or for spatial wind field modeling and estimation;
2) Sensors to measure/estimate the UAV's orientation $[\phi, \theta, \psi]$, which are needed for coordinate transformations between the body frame and the NED frame;
3) Sensors to measure/estimate air triplets $[V, \alpha, \beta]$, which are required to solve wind triangulation and for coordinate transformations between the wind frame and the body frame;
4) Sensors to measure/estimate the UAV's inertial and dynamic response to wind and turbulence, including body frame accelerations $[a_x, a_y, a_z]$, body frame rotation rates $[p, q, r]$, and control surface deflections $[\delta_a, \delta_e, \delta_r]$ and thrust $[\delta_t]$.

A. Sensors for Position and Ground Speed Measurements

Currently, most of unmanned aircraft systems rely on the Global Positioning System (GPS) for localization. In fact, many GPS receivers can also provide accurate ground speed measurements $[V_n, V_e, V_d]$ by utilizing Doppler effect. Low cost GPS receivers used on most small UAVs have an update rate within the range of 5 - 10 Hz and with the accuracy of a couple of meters. There are several ways to improve the accuracy of GPS, including sensor fusion with multi GPS antennas, real-time kinematic (RTK), real-time precise point positioning (PPP), and GNSS/INS fusion [31]. A typical differential GPS setup can achieve centimeter level accuracy, however, is usually more expensive. Comparisons of several typical GPS receivers are shown in Table 1.

B. Sensors for Attitude Estimation

Most UAVs nowadays rely on inertial measurement units (IMUs) for inertial measurements and attitude estimation. A typical MEMS IMU consists 3-axis accelerometers, 3-axis rate gyros, and 3-axis magnetometers. Accelerometers are used to measure translational accelerations $[a_x, a_y, a_z]$, rate gyros are used to measure rotation rates $[p, q, r]$, magnetometers are used to measure the magnetic field mostly for heading ψ correction. Attitudes $[\phi, \theta, \psi]$ of UAVs are

Table 1 Comparison of typical GPS receivers

	Horizontal Position Accuracy (CEP)	Velocity Accuracy	Heading Accuracy	Max Update Rate	Approximate Cost
Ublox LEA-6H	2.5 m	0.1 m/s	0.5 deg	5 Hz	90 USD
Ublox NEO-M8P	2.5 m	0.05 m/s	0.3 deg	10 Hz	150 USD
Ublox NEO-M8P RTK	0.025 m + 1 ppm	-	-	8 Hz	300 USD
NovAtel OEM615	1.5 m	0.03 m/s	-	50 Hz	1600 USD
NovAtel OEM615 RTK	0.01 m + 1 ppm	-	-	50 Hz	- USD

often estimated by combining multiple raw IMU measurements to compensate for sensor noises and drifts at an update rate of 50 - 100 Hz. It is typically done by integrating $[p, q, r]$ using Eq. (24)

$$\begin{bmatrix} \dot{\phi} \\ \dot{\theta} \\ \dot{\psi} \end{bmatrix} = \begin{bmatrix} 1 & \sin\phi\tan\theta & \cos\phi\tan\theta \\ 0 & \cos\phi & -\sin\phi \\ 0 & \frac{\sin\phi}{\cos\theta} & \frac{\cos\phi}{\cos\theta} \end{bmatrix} \begin{bmatrix} p \\ q \\ r \end{bmatrix}, \tag{24}$$

and combining with other measurements, such as accelerometers and magnetometers. Specifications of several widely used MEMS IMU based attitude and heading reference systems (AHRS) are shown in Table 2. Besides IMUs, there are vision-based systems to determine UAVs attitude [32].

Table 2 Comparison of AHRS

	Attitude Accuracy (Static: Typical)	Attitude Accuracy (Dynamic: Typical)	Update Rate	Approximate Cost
Pixhawk Cube (InvenSense) (MPU-9250)	-	-	Logged at 25 Hz by Default	200 USD
VectorNav-100	±0.5 deg (Roll, Pitch) ±2 deg (Yaw)	±1 deg (Roll, Pitch) ±2 deg (Yaw)	400 Hz	800 USD
MicroStrain 3DM-GX3-35	±0.5 deg (Roll, Pitch, Yaw)	±2 deg (Roll, Pitch, Yaw)	1000 Hz	1900 USD
MicroStrain 3DM-GX4-25	±0.25 deg (Roll, Pitch) ±0.8 deg (Yaw)	±0.25 deg (Roll, Pitch) ±0.8 deg (Yaw)	500 Hz	1600 USD
Xsense MTi -200 VRU	±0.2 deg (Roll, Pitch)	±0.3 deg (Roll, Pitch)	2000 Hz	3000 USD

C. Sensors for 3D Airspeed Measurements

3D airspeed vector $[u, v, w]$ or air triplets $[V, \alpha, \beta]$ describe the relative motion between UAVs and surrounding air. They are essential for wind/turbulence sensing and estimation. The airspeed V is generally measured by a Pitot-tube with pressure sensors attached. AOA/α and AOS/β can be directly measured using air flow sensors, such as flow vanes

or multi-hole Pitot-tubes. A flow vane, also known as a pivoted vane, is a mass-balanced wind vane that can align itself with the direction of the incoming air flow [33]. The angle between a flow vane and the reference line on the aircraft can then be measured by a potentiometer. Multi-hole Pitot-tubes can measure flow angles by sensing the pressure difference from different holes [33]. Specifications of several representative ADS are shown in Table 3. Note that there are other commercial vane sensors available on the market made by Space Age Control, Spingarage, etc, but these sensors have limited application on small UAVs due to their size and/or weight. There also exist other direct measurement methods, such as distributed pressure sensing [34, 35], optical sensors [36, 37], hot film sensors [38]. Recently, sonic anemometers have been installed on UAVs for wind measurements/estimation [39, 40].

Table 3 Comparison of ADS

	Airspeed/Pressure Accuracy	AOA/AOS Accuracy	Update Rate	Approximate Cost
MPXV7002 (Analog)	100 Pascal	-	Analog	30 USD
Eagle Tree Airspeed MicroSensor V3	NA (Resolution: 0.45 m/s)	-	50 Hz	60 USD
US Digital MA3 Encoder	-	-	250 Hz	50 USD
STI22FS Potentiometer (Analog)	-	-	Analog	150 USD
Aeroprobe Micro ADS	1 m/s (Range: 8 - 45 m/s)	±1 deg (Range: ±20 deg)	100 Hz	4500 USD

D. Sensors to Measure UAV's Dynamic Response to Wind

To study the interactions between UAVs and flow fields, especially UAV's dynamic response, it is important to measure the UAV's inertial states $[a_x, a_y, a_z]$ and $[p, q, r]$, which oftentimes by IMUs. The inertial and air flow angle measurements of an aircraft are usually good indicators of turbulence encounters, which are essentially the output of the aircraft open or closed loop system in response to wind disturbance. To single out the dynamic response due to flow fields, it is important to remove dynamic response caused by control surface maneuvers by using identified aircraft dynamic models. Most of small UAVs utilize pulse width modulation (PWM) signals to control actuators. Those PWM signals are generally logged during the flight and can be mapped to control surface deflection angles after offline calibrations. For example, control surface deflections $[\delta_a, \delta_e, \delta_r]$ can be obtained by attaching potentiometers to the control linkages. Thrust δ_t can be calculated using logged PWM signals and identified engine thrust model.

IV. Effects of Wind on UAV Motion

As mentioned in the previous section, certain sensors can be used to measure UAV's dynamic response to different flow fields. In order to estimate/reconstruct wind from sensor measurements, it is important to study the interaction between UAVs and wind and understand how wind affects UAV kinematics and dynamics. For manned aircraft, the effect of winds is more critical during takeoff or approach and landing at low altitudes, while the influence of winds is

not so important at high altitudes and speeds [7]. For small UAVs, the wind effect could be significant during all the stages of flight including cruise conditions [8, 41]. The effect of wind on UAV motion can be modeled generally in three ways, 1) point lift, 2) state space model, 3) distributed lift [7].

A. Wind Effect on UAV Motion (Point Lift)

When the changes of mean wind are sufficiently small with respect to the size of the UAV, all the aerodynamic forces can be concentrated at the center of gravity for analysis, which is called point lift [7]. The mean wind, gust, and turbulence affect the UAV motion through the body frame air speed vector ($[u, v, w]$ or $[V, \alpha, \beta]$) and the aerodynamic forces. Gust and turbulence also affect the UAV rotational motion including the rotation rate vector ($[p, q, r]$), and the rolling, pitching, and yawing moments. The body frame air speed vector can be written as [1]

$$\begin{bmatrix} u \\ v \\ w \end{bmatrix} = \begin{bmatrix} u' \\ v' \\ w' \end{bmatrix} - \begin{bmatrix} u_{\mathrm{w}} \\ v_{\mathrm{w}} \\ w_{\mathrm{w}} \end{bmatrix} = \begin{bmatrix} u' \\ v' \\ w' \end{bmatrix} - \boldsymbol{R}_{\boldsymbol{n}}^{\boldsymbol{b}}(\phi, \theta, \psi) \begin{bmatrix} \mathrm{w}_{n_s} \\ \mathrm{w}_{e_s} \\ \mathrm{w}_{d_s} \end{bmatrix} - \begin{bmatrix} u_{\mathrm{w}_t} \\ v_{\mathrm{w}_t} \\ w_{\mathrm{w}_t} \end{bmatrix}, \tag{25}$$

where $[u', v', w']$ are the ground speed expressed in the aircraft body frame, $[u_{\mathrm{w}}, v_{\mathrm{w}}, w_{\mathrm{w}}]$ are the wind speed in the aircraft body frame, $[\mathrm{w}_{n_s}, \mathrm{w}_{e_s}, \mathrm{w}_{d_s}]$ are slowly evolving wind in the NED frame, and $[u_{\mathrm{w}_t}, v_{\mathrm{w}_t}, w_{\mathrm{w}_t}]$ are turbulence disturbances expressed in the body frame.

Given estimated $[u, v, w]$, the airspeed magnitude and two flow angles can be derived using Eq. (26)

$$\begin{bmatrix} V \\ \alpha \\ \beta \end{bmatrix} = \begin{bmatrix} \sqrt{u^2 + v^2 + w^2} \\ \tan^{-1}(\frac{w}{u}) \\ \sin^{-1}(\frac{v}{\sqrt{u^2+v^2+w^2}}) \end{bmatrix}, \tag{26}$$

and then used for 3D wind estimation.

Note that the air triplets $[V, \alpha, \beta]$ affect the lift, drag, and thrust forces as well as rolling, pitching, and yawing moments. This means that the wind, gust, and turbulence effect will show up on the aerodynamic forces and accelerometer measurements, shown in Eq. (8). For example, the inertial sensors and airspeed magnitude can be combined for the estimation of inertial angle of attack and then the 3D wind [42, 43], assuming certain stability and control derivatives are known.

Gust and turbulence also affect the rotational motion, which can be modeled as gust induced rotational rate [19, 44]

$$\begin{bmatrix} p \\ q \\ r \end{bmatrix} = \begin{bmatrix} p_r \\ q_r \\ r_r \end{bmatrix} + \begin{bmatrix} p_\mathrm{t} \\ q_\mathrm{t} \\ r_\mathrm{t} \end{bmatrix}, \tag{27}$$

where $[p, q, r]$ are inertial rotational rates of the aircraft, $[p_r, q_r, r_r]$ are air-relative rotational rates of the aircraft, and $[p_t, q_t, r_t]$ are rotational rates of the turbulence. The gust and turbulence effect may show up on the UAV orientation angles, dependent on the disturbance magnitude and controller performance.

B. State Space Models with Turbulence Disturbance

Alternatively, state space aircraft longitudinal and lateral models can be used to include the wind impact, especially the turbulence impact on UAVs. A general state space model for UAV longitudinal or lateral dynamics is shown in Eq. (28) as an example [2, 45]. The longitudinal state space model has been used for the reconstruction of wind and turbulence in simulations [44].

$$\dot{\mathbf{x}} = \mathbf{A}\mathbf{x} + \mathbf{B}\mathbf{u} + \mathbf{G}\mathbf{w_t}, \tag{28}$$

where $\mathbf{x}$ is a vector of the longitudinal or lateral system states, $\mathbf{u}$ is a vector of the control surface deflections, $\mathbf{w_t}$ is a vector of the wind disturbances including $[u_{\mathrm{w}_t}, v_{\mathrm{w}_t}, w_{\mathrm{w}_t}, p_t, q_t, r_t]$.

The longitudinal state space model to describe the wind turbulence effect can be written as [2, 45]

$$\begin{bmatrix} \Delta\dot{u} \\ \Delta\dot{w} \\ \Delta\dot{q} \\ \Delta\dot{\theta} \end{bmatrix} = \begin{bmatrix} X_u & X_w & 0 & -g \\ Z_u & z_w & u_0 & 0 \\ M_u & M_w & M_q & 0 \\ 0 & 0 & 1 & 0 \end{bmatrix} \begin{bmatrix} \Delta u \\ \Delta w \\ \Delta q \\ \Delta\theta \end{bmatrix} + \begin{bmatrix} X_{\delta_e} & X_{\delta_t} \\ Z_{\delta_e} & Z_{\delta_t} \\ M_{\delta_e} & M_{\delta_t} \\ 0 & 0 \end{bmatrix} \begin{bmatrix} \delta_e \\ \delta_t \end{bmatrix} + \begin{bmatrix} -X_u & -X_w & 0 \\ -Z_u & -Z_w & 0 \\ -M_u & -M_w & -M_q \\ 0 & 0 & 0 \end{bmatrix} \begin{bmatrix} u_{\mathrm{w}_t} \\ w_{\mathrm{w}_t} \\ q_t \end{bmatrix}, \tag{29}$$

where $\Delta u, \Delta w, \Delta q, \Delta\theta$ are perturbed aircraft longitudinal states, $[\delta_e, \delta_t]$ are elevator and thrust control commands, $[u_{\mathrm{w}_t}, w_{\mathrm{w}_t}, q_t]$ is the longitudinal turbulence perturbation vector, $[X_u, ..., X_{\delta_t}]$, $[Z_u, ..., Z_{\delta_t}]$, and $[M_u, ..., M_{\delta_t}]$ are longitudinal stability and control derivatives of the aircraft. In simulations, u_{w_t}, w_{w_t}, and q_t are usually generated using Dryden turbulence model, shown in Eqs. (10)-(15).

Similarly, the lateral state space model to describe the wind turbulence effect can written as [2, 45]

$$\begin{bmatrix} \Delta\dot{v} \\ \Delta\dot{p} \\ \Delta\dot{r} \\ \Delta\dot{\phi} \end{bmatrix} = \begin{bmatrix} Y_v & 0 & (Y_r - u_0) & g \\ L_v & L_p & L_r & 0 \\ N_v & N_p & N_r & 0 \\ 0 & 1 & 0 & 0 \end{bmatrix} \begin{bmatrix} \Delta v \\ \Delta p \\ \Delta r \\ \Delta\phi \end{bmatrix} + \begin{bmatrix} 0 & Y_{\delta_r} \\ L_{\delta_a} & L_{\delta_r} \\ N_{\delta_a} & N_{\delta_r} \\ 0 & 0 \end{bmatrix} \begin{bmatrix} \delta_a \\ \delta_r \end{bmatrix} + \begin{bmatrix} -Y_v & 0 & 0 \\ -L_v & -L_p & -L_r \\ -N_v & -N_p & -N_r \\ 0 & 0 & 0 \end{bmatrix} \begin{bmatrix} v_{\mathrm{w}_t} \\ p_t \\ r_t \end{bmatrix}, \quad (30)$$

where $\Delta v, \Delta p, \Delta r, \Delta\phi$ are perturbed aircraft longitudinal states, $[v_{\mathrm{w}_t}, p_t, r_t]$ are lateral turbulence perturbation vectors, $[\delta_a, \delta_r]$ are aileron and rudder commands, $[Y_v, ..., Y_{\delta_r}]$, $[L_v, ..., L_{\delta_r}]$, and $[N_v, ..., N_{\delta_r}]$ are lateral stability and control derivatives of the aircraft. In simulations, v_{w_t}, p_t, and r_t can be generated using Dryden turbulence model [1].

C. Wind Effect on UAV Motion (Distributed Lift)

Although UAV-wind interaction can be modeled by single point force analysis, the accuracy of which is often limited as these dynamics equations are only accurate under nominal cases (under small perturbation assumptions). Instead of analyzing the aircraft forces only through one point, a general computational approach is to consider multiple grids on the aircraft for force and moment analysis [45, 46]. The wind impact modeling can be improved by incorporating aerodynamic changes into flight dynamics, which is usually calculated using CFD models. The impact of nonuniform flow field on UAVs will show up in the aerodynamic forces and moments including lift, drag, thrust, rolling moment, pitching moment, and yawing moment. CFD methods can be used to calculate these forces and moments given the nonuniform wind field information. A good example is the prediction of wake vortex influence on aircraft responses using vortex lattice method during aircraft wake vortex encounters [46, 47]. The wake induced aerodynamic forces and moments can be combined with the forces and moments from the mean wind to predict the aircraft inertial responses including rotation rates, orientations, accelerations, velocities, and positions.

V. Summaries of Existing Work and Recommendations

In this section, representative solutions for wind sensing and estimation using fixed-wing UAVs are summarized. General recommendations and considerations are provided to help determine which wind models, sensors, and algorithms are needed for future research related to wind sensing and estimation.

A. Summary of Existing Work

Representative works for wind sensing and estimation using fixed-wing UAVs are summarized in Table 4 with the main focus on those with flight validation results. Different combinations of sensor hardware and estimation filters are shown in the table as well. Note that references shown in *emph* are with simulation results only, while references shown

in **bold** have flight test results. In addition, in some references, results from multiple methods are presented.

Table 4 Existing work on wind sensing and estimation using small fixed-wing UAVs

	GPS	IMU + GPS	GPS + Regular Pitot-Tube	IMU+GPS+ Regular Pitot-Tube	IMU+GPS+ Regular Pitot-Tube+ Mechanical Vanes	IMU+GPS+ Multi-Hole Pitot-Tube	IMU+GPS+ Sonic Anemometer	Other
Direct/MAF					3D prevailing **[48]**	2D prevailing **[49–51]** 3D prevailing *[52]* **[53]** PSD **[54, 55]**	2D prevailing **[39]**	
EKF		1st-Order RW: 2D prevailing **[56]**	1st-Order RW: 2D prevailing **[57]** 3D prevailing *[60]*	1st-Order RW: 2D prevailing **[50, 58]** 3D prevailing *[61]* **[43, 48]** Thermal Model: Updraft estimation **[63]**	1st-Order RW: 3D prevailing **[59]**			1st-Order RW 2D prevailing Vision+Regular Pitot-Tube **[62]**
UKF			1st-Order RW: 2D prevailing **[64]** 3D prevailing **[64]**	1st-Order RW + Dryden: 3D prevailing + turbulence **[66]**	1st-Order RW: 3D prevailing **[64, 65]** 2nd-Order RW: 3D prevailing **[67]**			
PF						Thermal Model: Updraft estimation *[68]*		
Others	2D prevailing wind **[50, 69, 70]**			1st-Order RW + Dryden: 3D prevailing **[18]**				

Most of the existing algorithms can be divided into two broad categories, deterministic algorithms, which include the moving average filter (MAF) and the complementary filter (CF), and stochastic algorithms, which include the extended Kalman filter (EKF), the unscented Kalman filter (UKF), and the particle filter (PF). Deterministic algorithms are usually more computationally efficient and easier to implement. However, they lack the ability to handle unknown noises and biases. On the other hand, the tuning of the stochastic filter can be quite challenging for different noise parameters [10]. Because small UAVs are often limited by budget and payload, stochastic algorithms are more often used for more accurate results. Other than the algorithms mentioned above, there are other algorithms that can be applied to the wind estimation problem, such as optimization based approach (for example, model predictive control) [71], fuzzy logic and data driven approach (for example, neural network and machine learning) [72, 73].

It is shown in Table 4 that the combination of EKF and 1st-order RW model is the most popular formulation for UAV-based wind estimation as such a combination is easy to implement and computational friendly. This combination has also been shown to be reasonably effective, even with respect to more complicated models [11, 12]. In addition, 2D prevailing wind can be accurately estimated using only IMU and GPS or even GPS by itself with support from optimization methods [69, 70]. However, UAVs are required to perform certain maneuvers, such as circling (roll/pitch/heading change), to make wind states observable [74, 75]. A standard setup for 2D prevailing wind estimation is GPS + regular Pitot-tube

[57] or IMU + GPS + regular Pitot-tube [58]. For the problem of 3D wind sensing/estimation, most of the existing work requires direct measurements of air triplets either using a regular Pitot-tube and flow angle vanes or a multi-hole Pitot-tube [53]. However, if certain assumptions regarding AOA and AOS are made [48] or partial UAV aerodynamic model is available [43, 66], it is possible to estimate 3D wind with the set up of IMU, GPS, and a regular Pitot-tube. Generally speaking, more direct wind measurements will improve the observability and redundancy of a filter, however, it is not required to have all measurements for a filter to work. For example, some states or measurements like AOA or AOS can be derived instead of directly measured if UAV dynamics models are known [56]. The observability issue can also be tackled by performing certain maneuvers [74, 75].

For meteorological applications, most researchers used direct calculation methods and are interested in vertical wind profile and the PSD of wind field. On the other side, most researchers in robotics or guidance, navigation, and control community often used stochastic filters for mean wind estimation, with few applications using direct flow angle measurements (aircraft wake encounters). The reason is that most of the small UAVs nowadays are already equipped with GPS and IMU since they are cheap, light weight, and widely available. But very few UAVs are equipped with a high quality ADS.

Another major challenge for UAV based wind estimation comes from the validation and estimation error quantification part, since it is difficult to find a ground truth of the spatio-temporal wind field around an UAV during flight tests. A widely used method for validation is comparing UAV wind estimation results with measurements from other wind sensing instruments such as ground wind anemometer, SODAR, LiDAR, radiosonde, or a multi-hole probe based air data system onboard the same UAV. Among these instruments, ground wind anemometers are the mostly used, as they are relatively cheaper and easier to deploy. However, the major drawback is that they are often not at the same locations or altitude as UAVs. Therefore, measurements from ground weather stations need to be interpolated or extrapolated using certain wind profile models for fair comparisons with UAV wind estimates along the flight trajectory. A summary of ground truth source and UAV wind estimation error comparison from several representative papers are shown in Table 5. Note that there are also graph-based comparison results between UAV wind estimates and ground wind measurements with no error statistics [50, 59]. In summary, it can be observed from Table 5 and other literature that the ground truth source and the way of presentation are quite different, which makes it difficult to perform systematic performance comparison among different wind estimation filters. In addition, the selected ground truth data can also introduce nontrivial errors.

Since a great number of wind sensing and estimation solutions is Kalman filter based, several representative Kalman filter formulations are shown below. Note that as a survey paper, implementation details are not the focus. Only state, input, and measurement vectors for these representative Kalman filters are included in the following sections. Implementation details regarding the Kalman filter in general and these representative formulations can be found in [76] and [43, 57, 59, 64, 77], respectively.

Table 5 Wind estimation results from flight tests

	Ground Truth Source	Wind Estimation Results
[18]	Along-trajectory wind from a multi-hole probe and GPS/INS	RMSE of 3D wind estimation in body frame x, y, z (1 m/s, 1.8 m/s, 0.6 m/s)
[43]	Ground weather station with sonic anemometer (3 m) Power law corrected	3D wind estimation in NED frame N, E, D Mean error (0.88 m/s, 0.69 m/s, 0.84 m/s) Error standard deviation (0.80 m/s, 0.41 m/s, 0.70 m/s)
[48]	Along-trajectory wind from Pitot-tube, vane measurements,and GPS/INS	RMSE of 3D wind estimation in body frame x, y, z (0.13 m/s, 1.1 m/s, 1 m/s)
[49]	Sodar, Weather tower (99 m)	Mean horizontal wind speed error within 1 m/s Average direction error 20 deg Vertical wind standard deviations up to 0.4 m/s
[57]	Automatic weather station (15 km away) Power law corrected	Mean horizontal wind speed error 1.2 m/s Mean direction error 5.6 deg
[65]	Portable ground weather station (7 m) Power law corrected	Mean horizontal wind speed error 0.11 m/s Mean direction error 16.71 deg

1. Representative 2D Prevailing Wind Estimation Filter

Cho et. al. presented a simple extended Kalman filter (EKF) for the estimation of 2D horizontal wind using only a conventional Pitot-tube and a GPS receiver [57]. The EKF states, inputs, and measurements are shown in Eq. (31)

$$\mathbf{x} = [V_\mathrm{w} \;\; \psi_\mathrm{w} \;\; sf]^T, \tag{31a}$$

$$\mathbf{u} = [V_g \;\; \psi_g]^T, \tag{31b}$$

$$\mathbf{z} = [p_d]^T, \tag{31c}$$

where V_w is the wind speed, ψ_w is the wind direction, sf is the scaling factor for the pressure sensor, and p_d is the dynamic pressure. The propagation equations follow the first order random walk model. The measurement equation is:

$$V_g{}^2 + V_\mathrm{w}{}^2 - 2V_g V_\mathrm{w} \cos\left(\psi_\mathrm{w} - \psi_g\right) = V_a^2 = \frac{p_d}{sf}. \tag{32}$$

The wind triangle equation for this formulation is given by Eq. (32), where ψ_g is UAV heading calculated from GPS. Cho's filter is one of the simplest horizontal wind estimation filter for UAVs. It requires certain UAV maneuvers such as circling or figure 8 to meet the observability requirements.

2. Representative 3D Prevailing Wind Estimation Filter with Direct Flow Angle Measurements

Rhudy et. al. developed an UKF that could estimate aircraft attitude and 3D wind simultaneously using measurements from IMU, GPS, airspeed sensor, and flow angle vanes [64]. The UKF states, inputs, and measurements are shown in

Eq. (33)

$$\mathbf{x} = [u \;\; v \;\; w \;\; \phi \;\; \theta \;\; \psi \;\; \mathrm{w}_n \;\; \mathrm{w}_e \;\; \mathrm{w}_d]^T, \tag{33a}$$

$$\mathbf{u} = [a_x \;\; a_y \;\; a_z \;\; p \;\; q \;\; r]^T, \tag{33b}$$

$$\mathbf{z} = [V_n \;\; V_e \;\; V_d \;\; V_{pitot} \;\; \alpha \;\; \beta]^T. \tag{33c}$$

These states are propagated using Eq. (8), Eq. (24), and Eq. (5). The measurement equations are Eq. (1) and Eq. (3). Rhudy's filter combines conventional inertial, GPS, and flow angle measurements for accurate estimates of 3D wind. However, it may be difficult to install or maintain flow angle vanes on UAVs, especially flying wing UAVs.

3. Representative 3D Prevailing Wind Estimation Filter without Direct Flow Angle Measurements

To estimate 3D wind without direct flow angle measurements, certain assumptions regarding AOA and AOS have to be made. The assumptions can be either model-free [48], or model-aided [43]. The approach in [43] is based on an EKF, where the filter states, inputs, are the same with those shown in Eq. (33a) and Eq. (33b). However, the major difference between [64] and [43] is that instead of relying on direct flow angle measurements for update, [43] takes the model-aided approach by correlating lift equations and side force equations with inertial angles of attack and sideslip.

4. Tightly Coupled Navigation and Wind Estimation Filter

There are other formulations to solve the wind triangle equation through tightly coupled filters with many other aircraft states. For example, wind estimation can be coupled with UAV navigation states to form a tightly coupled EKF [59, 77]. A representative example for these types of filters is the EKF2 in the open source pixhawk codebase [77]. The EKF states, inputs, and measurements are shown in Eq. (34)

$$\mathbf{x} = [q_0 \;\; q_1 \;\; q_2 \;\; q_3 \;\; V_n \;\; V_e \;\; V_d \;\; P_n \;\; P_e \;\; P_d \;\; p_b \;\; q_b \;\; r_b \;\; a_{x_b} \;\; a_{y_b} \;\; a_{z_b} \;\; M_n \;\; M_e \;\; M_d \;\; M_x \;\; M_y \;\; M_z \;\; \mathrm{w}_n \;\; \mathrm{w}_e]^T, \tag{34a}$$

$$\mathbf{u} = [a_x \;\; a_y \;\; a_z \;\; p \;\; q \;\; r]^T, \tag{34b}$$

$$\mathbf{z} = [V_{n_m} \;\; V_{e_m} \;\; V_{d_m} \;\; P_{n_m} \;\; P_{e_m} \;\; P_{d_m} \;\; M_{x_m} \;\; M_{y_m} \;\; M_{z_m} \;\; V_m \;\; \psi_m \;\; \beta_m]^T, \tag{34c}$$

where $[q_0, q_1, q_2, q_3]$ are attitude quaternions, $[p_b, q_b, r_b]$ are gyro biases, $[a_{x_b}, a_{y_b}, a_{z_b}]$ are accelerometer biases, $[M_n, M_e, M_d]$ is the earth magnetic field, $[M_x, M_y, M_z]$ is the body magnetic field, and $_m$ denotes the measurement. The propagation equations and measurement equations follow standard aircraft equations of motion [1, 77]. Note that in the observation innovations, yaw angle ψ_m and sideslip angle β_m are optional and may not be direct measurements. For example, ψ_m can be calculated from GPS velocities whereas β_m is typically assumed to be zero for fixed-wing UAVs. Measurements from optical flow sensor and barometer can also be used.

B. Recommendations for Wind Model, Sensor, and Algorithm

The two most important factors to consider for UAV-based wind sensing and estimation are the application scenario and budget, which can help determine what platform, wind models, and sensors to use. Consequently, those selected wind models and sensors will help determine the type of estimation filters. For example, for thermal soaring missions, it is straightforward to use a glider equipped with GPS, IMU, and ADS. If resources are available, a full ADS with accurate AOA and AOS measurements can be used, with the help from certain vertical wind estimation algorithms. If the budget or payload is limited, a low cost system with the conventional Pitot-tube can be selected instead. The first order RW model and the thermal model can be used to represent wind dynamics in an EKF or UKF sensor fusion framework. In summary, it is important to find a balance between hardware/sensors and software/algorithms as well as between cost and performance accuracy. A good overview of UAV platforms and sensors for meteorological sampling can be found in [3].

General considerations and recommendations regarding wind model, sensor, and algorithm selection are listed as follows.

For the selection of wind models, it is crucial to identify the dominant wind component to be measured or estimated. For general UAV wind sensing and estimation problems, a combination of several wind models including prevailing wind, turbulence, and wind shear may yield the best results. It is also important to think about how to incorporate wind models into flight dynamic models, as different modeling methods can affect estimation accuracy differently, especially under turbulent conditions [44].

For the selection of sensors, the following major points need to be considered:

1) Sensor type and budget: The major wind measurement sensor onboard a UAV needs to be carefully selected based on the application focus and budget. For instance, a high quality airflow angle sensor such as a multi-hole probe is usually selected for many meteorological turbulence measurement scenarios [54, 55], while an accurate IMU is more important for gust alleviation control application;
2) Size and weight: UAVs, especially small UAVs are often limited by their space and weight. Small and light sensors with low power consumption are usually preferred for small UAVs due to installation challenges [3];
3) Update rate: Sensor and filter update rate needs to be carefully evaluated based on frequencies of interest for the targeted wind field. For example, sensors with a high update rate (50 - 100 Hz or higher) need to be selected for turbulence measurement applications [53, 55];
4) Estimation accuracy: Although delicately designed algorithms/filters can improve the estimation accuracy, it is essentially limited by the accuracy of sensor measurements [3, 52];
5) Noise level: Filters are often required for low cost sensors with a high random noise level. The low signal to noise ratio will make it difficult for the signal reconstruction;
6) Location of installation: Locations of wind sensors are critical to later modeling and control efforts. For example,

the location and orientation alignment of an IMU is critical to the wind speed transformation from the body frame to the inertial frame as well as to the aircraft system identification and flight control. Another good example is the ADS, where the Pitot-tube should be installed far enough from the fuselage to stay away from the structure generated disturbance. The location of flow angle vanes also have a big impact on the sensor calibration and turbulence detection such as wake vortices [78].

For the selection of wind estimation algorithms, the following questions need to be answered:

1) Can you afford a suite of high quality airflow sensors for your UAV both budget wise and payload wise? If yes, the most accurate and reliable sensors can be selected with the highest update rate within your budget. Otherwise, aerodynamic model-aided filters [43, 56] or optimization approaches [79] can be used to compensate for the missing of direct flow measurements;
2) How is your sensor quality and calibration? Are your sensor noises/biases/alignment errors small? If yes, deterministic algorithms such as MAF or CF can be used. Otherwise, stochastic algorithms are usually preferred;
3) What is your computational power constraint? CFs and EKFs are generally considered computationally efficient while UKFs, PFs, and optimization based approaches are often computationally intensive for most UAVs' onboard microprocessors;
4) Are you planning to reuse an existing estimation framework? If yes, cascaded filter structure can be utilized [56, 58, 61]; Otherwise, a tightly coupled filter structure can be implemented [59];
5) How is the observability of the developed filter/algorithm? Certain flight maneuvers may be required for filter convergence [70, 74, 75];
6) Are you interested in both wind speed estimation and wind field estimation? If yes, parameters in the wind field model can be implemented as states in the filter/algorithm to be estimated [80–82].

C. Potential Future Directions for Wind Estimation

In summary, there are many challenges for UAV-based wind estimation such as sensor, filter, and model selection, and wind validation truth. The following potential future directions are envisioned for wind estimation problem:

1) Turbulence estimation: Current state of the art wind estimation filters are mostly for prevailing wind estimation. There exist aircraft-based turbulence estimation approaches from meteorological society. For example, energy dissipation rate (EDR) estimation [83]. However, direct flow measurements such as flow vanes or multi-hole probe are usually required. It will be very useful if aerodynamic model-aided filters can be developed for UAV-based turbulence estimation;
2) Further analysis on observability and convergence of the wind estimation filters: Current Kalman filter based approaches for wind estimation usually use the 1st order RW based wind model. However, the wind field pattern for UAV BVLOS operations could be quite different both spatially or temporally. It is unclear if the filter estimate

can converge and how fast it can converge given highly dynamic wind fields;

3) Wind field pattern estimation: Most of the existing literature focuses on wind estimation along the aircraft trajectory. There may exist strong spatial or temporal patterns for a specific wind field such as fire generated plumes or flows around a building. It will be very useful to consider those temporal or spatial wind patterns in design of low-level flight control or high-level guidance law;
4) Performance quantification for UAV based wind sensing system: Although many researchers have developed different UAVs for wind and turbulence sensing missions, the overall system performance requirements are not well quantified including accuracy, dynamic response, full-scale range, etc.
5) Wind field prediction: To improve flight performance and safety, it will be beneficial if the wind field ahead can be predicted or interpolated based on previous wind estimates along the UAV trajectory or from neighboring aircraft. Examples include thermal prediction and wake vortex prediction and sensing.

VI. Conclusions

This paper presents a thorough survey of existing methods on wind sensing and estimation using small fixed-wing UAVs. Representative wind models are first introduced for the wind sensing and estimation problem. Available UAV sensors are then summarized and compared, with the focus on UAV dynamic responses to wind and turbulence. Representative stochastic filter types and formulations are discussed and compared in detail with recommendations for future research directions. Through the summary of existing work, it is found that the selection of wind measurement and estimation methods are primarily driven by applications. For example, researchers working on meteorological applications tend to use direct calculation methods with a complete and high quality sensor suite (e.g., a multi-hole probe) while researchers working on GNC applications prefer stochastic filters with a standard sensor suite. In addition, the EKF is the most popular filter for small UAV-based wind estimation, whereas the 1st-order RW model is the most widely used wind model. The majority of existing work focuses on the time domain prevailing wind estimation, where 2D prevailing wind estimation is well studied and available on open source autopilots. In the past several years, researchers started to work on 3D prevailing wind estimation without using direct flow angle measurements. Future wind estimation researches for fixed-wing UAVs may focus on turbulence estimation, enhanced wind modeling, wind field estimation, and wind field prediction.

Acknowledgments

This work was partially supported by the University of Kansas General Research Fund allocation #2221800 and USDA-NIFA Grant 2019-67021-28992.

References

[1] Beard, R. W., and McLain, T. W., *Small Unmanned Aircraft: Theory and Practice*, Princeton University Press, 2012. https://doi.org/10.1515/9781400840601.

[2] Nelson, R. C., et al., *Flight Stability and Automatic Control*, Vol. 2, WCB/McGraw Hill New York, 1998. https://doi.org/10.1017/S0001924000065362.

[3] Elston, J., Argrow, B., Stachura, M., Weibel, D., Lawrence, D., and Pope, D., "Overview of Small Fixed-Wing Unmanned Aircraft for Meteorological Sampling," *Journal of Atmospheric and Oceanic Technology*, Vol. 32, No. 1, 2015, pp. 97–115. https://doi.org/10.1175/jtech-d-13-00236.1.

[4] Abichandani, P., Lobo, D., Ford, G., Bucci, D., and Kam, M., "Wind Measurement and Simulation Techniques in Multi-Rotor Small Unmanned Aerial Vehicles," *IEEE Access*, Vol. 8, 2020, pp. 54910–54927. https://doi.org/10.1109/access.2020.2977693.

[5] Neumann, P. P., and Bartholmai, M., "Real-Time Wind Estimation on a Micro Unmanned Aerial Vehicle Using Its Inertial Measurement Unit," *Sensors and Actuators A: Physical*, Vol. 235, 2015, pp. 300–310. https://doi.org/10.1016/j.sna.2015.09.036.

[6] Stull, R. B., *An Introduction to Boundary Layer Meteorology*, Vol. 13, Springer Science & Business Media, 1988. https://doi.org/10.1007/978-94-009-3027-8.

[7] Barr, N. M., Gangsaas, D., and Schaeffer, D. R., "Wind Models for Flight Simulator Certification of Landing and Approach Guidance and Control Systems," Tech. rep., BOEING COMMERCIAL AIRPLANE CO SEATTLE WA, 1974.

[8] Cole, K., and Wickenheiser, A., "Spatio-Temporal Wind Modeling for UAV Simulations," *arXiv*, 2019, pp. arXiv–1905.

[9] National Weather Service, "Turbulence," , 2020. URL https://www.weather.gov/source/zhu/ZHU_Training_Page/turbulence_stuff/turbulence/turbulence.htm.

[10] Rhudy, M. B., "Predicting the Parameters of Stochastic Wind Models for Time-Varying Wind Estimation Techniques," *Journal of Aerospace Information Systems*, Vol. 16, No. 2, 2019, pp. 71–76. https://doi.org/10.2514/1.i010652.

[11] Rhudy, M. B., Fravolini, M. L., Porcacchia, M., and Napolitano, M. R., "Comparison of Wind Speed Models within a Pitot-Free Airspeed Estimation Algorithm Using Light Aviation Data," *Aerospace Science and Technology*, Vol. 86, 2019, pp. 21–29. https://doi.org/10.1016/j.ast.2018.12.028.

[12] Rhudy, M. B., Gross, J. N., and Gu, Y., "Stochastic Wind Modeling and Estimation for Unmanned Aircraft Systems," *AIAA Aviation 2019 Forum*, 2019, pp. AIAA Paper 2019–3111. https://doi.org/10.2514/6.2019-3111.

[13] Negra, N. B., Holmstrøm, O., Bak-Jensen, B., and Sørensen, P., "Model of a Synthetic Wind Speed Time Series Generator," *Wind Energy: An International Journal for Progress and Applications in Wind Power Conversion Technology*, Vol. 11, No. 2, 2008, pp. 193–209. https://doi.org/10.1002/we.244.

[14] Shamshad, A., Bawadi, M., Hussin, W. W., Majid, T., and Sanusi, S., "First and Second Order Markov Chain Models for Synthetic Generation of Wind Speed Time Series," *Energy*, Vol. 30, No. 5, 2005, pp. 693–708. https://doi.org/10.1016/j.energy.2004.05.026.

[15] Hoblit, F. M., *Gust Loads on Aircraft: Concepts and Applications*, AIAA Education Series, AIAA, Reston, VA, 1988. https://doi.org/10.2514/4.861888.

[16] U.S. Military Specification, *MIL-F-8785C*, 1980.

[17] U.S. Military Handbook, *MIL-HDBK-1797*, 1997.

[18] Wenz, A., and Johansen, T. A., "Moving Horizon Estimation of Air Data Parameters for UAVs," *IEEE Transactions on Aerospace and Electronic Systems*, Vol. 56, No. 3, 2020, pp. 2101–2121. https://doi.org/10.1109/taes.2019.2946677.

[19] MathWorks, "Dryden Wind Turbulence Model (Continuous)," , 2020. URL https://www.mathworks.com/help/aeroblks/drydenwindturbulencemodelcontinuous.html.

[20] MathWorks, "Von Karman Wind Turbulence Model (Continuous)," , 2020. URL https://www.mathworks.com/help/aeroblks/vonkarmanwindturbulencemodelcontinuous.html.

[21] Oke, T. R., *Boundary Layer Climates*, Routledge, 2002. https://doi.org/10.4324/9780203407219.

[22] Gedeon, J., "Dynamic Analysis of Dolphin-Style Thermal Cross-Country Flight: Part II," *Technical Soaring*, Vol. 3, No. 3, 1973, pp. 17–34.

[23] Touma, J. S., "Dependence of the Wind Profile Power Law on Stability for Various Locations," *Journal of the Air Pollution Control Association*, Vol. 27, No. 9, 1977, pp. 863–866. https://doi.org/10.1080/00022470.1977.10470503.

[24] Holmes, J. D., *Wind Loading of Structures*, CRC Press, 2018. https://doi.org/10.1201/b18029.

[25] Burnham, D., and Hallock, J., "Chicago Monostatic Acoustic Vortex Sensing System. Volume IV. Wake Vortex Decay." Tech. rep., Transportation systems Center Cambridge MA, 1982.

[26] Larrabee, T., Chao, H., Rhudy, M., Gu, Y., and Napolitano, M. R., "Wind Field Estimation in UAV Formation Flight," *2014 American Control Conference*, IEEE Pages 5408–5413, 2014. https://doi.org/10.1109/acc.2014.6859266.

[27] Sarpkaya, T., "New Model for Vortex Decay in the Atmosphere," *Journal of Aircraft*, Vol. 37, No. 1, 2000, pp. 53–61. https://doi.org/10.2514/2.2561.

[28] Pahle, J., Berger, D., Venti, M., Duggan, C., Faber, J., and Cardinal, K., "An Initial Flight Investigation of Formation Flight for Drag Reduction on the C-17 Aircraft," *AIAA Atmospheric Flight Mechanics Conference*, AIAA Paper 2012-4802, 2012. https://doi.org/10.2514/6.2012-4802.

[29] Oettershagen, P., Achermann, F., Müller, B., Schneider, D., and Siegwart, R., "Towards Fully Environment-Aware UAVs: Real-Time Path Planning with Online 3D Wind Field Prediction in Complex Terrain," *arXiv preprint arXiv:1712.03608*, 2017.

[30] Achermann, F., Lawrance, N. R., Ranftl, R., Dosovitskiy, A., Chung, J. J., and Siegwart, R., "Learning to Predict the Wind for Safe Aerial Vehicle Planning," *2019 International Conference on Robotics and Automation (ICRA)*, IEEE Pages 2311–2317, 2019. https://doi.org/10.1109/icra.2019.8793547.

[31] Watson, R. M., Gross, J. N., Bar-Sever, Y., Bertiger, W. I., and Haines, B. J., "Flight Data Assessment of Tightly Coupled PPP/INS Using Real-Time Products," *IEEE Aerospace and Electronic Systems Magazine*, Vol. 32, No. 8, 2017, pp. 10–21. https://doi.org/10.1109/maes.2017.160169.

[32] Demonceaux, C., Morel, O., Fofi, D., et al., "Vision Based UAV Attitude Estimation: Progress and Insights," *Journal of Intelligent & Robotic Systems*, Vol. 65, No. 1-4, 2012, pp. 295–308. https://doi.org/10.1007/s10846-011-9588-y.

[33] Gracey, W., "Summary of Methods of Measuring Angle of Attack on Aircraft," Tech. rep., Langley Aeronautical Laboratory, 1958.

[34] Whitmore, S. A., Davis, R. J., and Fife, J., "In-Flight Demonstration of a Real-Time Flush Airdata Sensing System," *Journal of Aircraft*, Vol. 33, No. 5, 1996, pp. 970–977. https://doi.org/10.2514/3.47043.

[35] Yeo, D., Henderson, J., and Atkins, E., "An Aerodynamic Data System for Small Hovering Fixed-Wing UAS," *AIAA Guidance, Navigation, and Control Conference*, AIAA Paper 2009-5756, 2009. https://doi.org/10.2514/6.2009-5756.

[36] McDevitt, T. K., and Owen, F. K., "An Optical Angle of Attack Sensor," *International Congress on Instrumentation in Aerospace Simulation Facilities*, IEEE Pages 113–124, 1989. https://doi.org/10.1109/iciasf.1989.77664.

[37] Strader, J., Harper, S., and Gu, Y., "Aircraft Instrumentation and Computer Vision-Aided Flight Analysis of Local Air Flow," *AIAA Flight Testing Conference*, AIAA Paper 2016-3653, 2016. https://doi.org/10.2514/6.2016-3653.

[38] Zhu, R., Liu, P., Liu, X., Zhang, F., and Zhou, Z., "A Low-Cost Flexible Hot-Film Sensor System for Flow Sensing and Its Application to Aircraft," *2009 IEEE 22nd International Conference on Micro Electro Mechanical Systems*, IEEE Pages 527–530, 2009. https://doi.org/10.1109/memsys.2009.4805435.

[39] Barthelmie, R., Crippa, P., Wang, H., Smith, C., Krishnamurthy, R., Choukulkar, A., Calhoun, R., Valyou, D., Marzocca, P., Matthiesen, D., et al., "3D Wind and Turbulence Characteristics of the Atmospheric Boundary Layer," *Bulletin of the American Meteorological Society*, Vol. 95, No. 5, 2014, pp. 743–756. https://doi.org/10.1175/bams-d-12-00111.1.

[40] Hollenbeck, D., Nunez, G., Christensen, L. E., and Chen, Y., "Wind Measurement and Estimation with Small Unmanned Aerial Systems (sUAS) Using On-Board Mini Ultrasonic Anemometers," *2018 International Conference on Unmanned Aircraft Systems (ICUAS)*, IEEE Pages 285–292, 2018. https://doi.org/10.1109/icuas.2018.8453418.

[41] Wang, B. H., Wang, D. B., Ali, Z. A., Ting Ting, B., and Wang, H., "An Overview of Various Kinds of Wind Effects on Unmanned Aerial Aehicle," *Measurement and Control*, Vol. 52, No. 7-8, 2019, pp. 731–739. https://doi.org/10.1177/0020294019847688.

[42] Tian, P., Chao, H., Flanagan, H. P., Hagerott, S. G., and Gu, Y., "Design and Evaluation of UAV Flow Angle Estimation Filters," *IEEE Transactions on Aerospace and Electronic Systems*, Vol. 55, No. 1, 2019, pp. 371–383. https://doi.org/10.1109/taes.2018.2852359.

[43] Tian, P., and Chao, H., "Model Aided Estimation of Angle of Attack, Sideslip Angle, and 3D Wind without Flow Angle Measurements," *AIAA Guidance, Navigation, and Control Conference*, AIAA Paper 2018-1844, 2018. https://doi.org/10.2514/6.2018-1844.

[44] McClelland, H. G., and Woolsey, C. A., "Effects of Two Modeling Assumptions on Wind Reconstruction from Longitudinal Aircraft Motion," *Journal of Guidance, Control, and Dynamics*, Vol. 43, No. 6, 2020, pp. 1069–1081. https://doi.org/10.2514/1.g004224.

[45] Etele, J., and Fusina, G., *Overview of Wind Gust Modelling with Application to Autonomous Low-Level UAV Control*, Defence R&D Canada, 2006.

[46] Tian, P., He, A., Chao, H., Zheng, Z. C., and Gu, Y., "Wake Encounter Simulation and Flight Validation with UAV Close Formation Flight," *AIAA Guidance, Navigation, and Control Conference*, AIAA Paper 2017-1910, 2017. https://doi.org/10.2514/6.2017-1910.

[47] Fischenberg, D., "A Method to Validate Wake Vortex Encounter Models from Flight Test Data," *27th International Congress of the Aeronautical Sciences*, ICAS 2010-6.9.1, 2010.

[48] Balmer, G., Muskardin, T., Wlach, S., and Kondak, K., "Enhancing Model-Free Wind Estimation for Fixed-Wing UAV," *2018 International Conference on Unmanned Aircraft Systems (ICUAS)*, IEEE Pages 1242–1247, 2018. https://doi.org/10.1109/icuas.2018.8453419.

[49] Van den Kroonenberg, A., Martin, T., Buschmann, M., Bange, J., and Vörsmann, P., "Measuring the Wind Vector Using the Autonomous Mini Aerial Vehicle M^2AV," *Journal of Atmospheric and Oceanic Technology*, Vol. 25, No. 11, 2008, pp. 1969–1982. https://doi.org/10.1175/2008jtecha1114.1.

[50] Rautenberg, A., Graf, M. S., Wildmann, N., Platis, A., and Bange, J., "Reviewing Wind Measurement Approaches for Fixed-Wing Unmanned Aircraft," *Atmosphere*, Vol. 9, No. 11, 2018, p. 422. https://doi.org/10.3390/atmos9110422.

[51] Niedzielski, T., Skjøth, C., Werner, M., Spallek, W., Witek, M., Sawiński, T., Drzeniecka-Osiadacz, A., Korzystka-Muskała, M., Muskała, P., Modzel, P., et al., "Are Estimates of Wind Characteristics Based on Measurements with Pitot Tubes and GNSS Receivers Mounted on Consumer-Grade Unmanned Aerial Vehicles Applicable in Meteorological Studies?" *Environmental monitoring and assessment*, Vol. 189, No. 9, 2017, p. 431. https://doi.org/10.1007/s10661-017-6141-x.

[52] Langelaan, J. W., Alley, N., and Neidhoefer, J., "Wind Field Estimation for Small Unmanned Aerial Vehicles," *Journal of Guidance, Control, and Dynamics*, Vol. 34, No. 4, 2011, pp. 1016–1030. https://doi.org/10.2514/6.2010-8177.

[53] Reineman, B. D., Lenain, L., and Melville, W. K., "The Use of Ship-Launched Fixed-Wing UAVs for Measuring the Marine Atmospheric Boundary Layer and Ocean Surface Processes," *Journal of Atmospheric and Oceanic Technology*, Vol. 33, No. 9, 2016, pp. 2029–2052. https://doi.org/10.1175/jtech-d-15-0019.1.

[54] Mohamed, A., Abdulrahim, M., Watkins, S., and Clothier, R., "Development and Flight Testing of a Turbulence Mitigation System for Micro Air Vehicles," *Journal of Field Robotics*, Vol. 33, No. 5, 2016, pp. 639–660. https://doi.org/10.1002/rob.21626.

[55] Reuder, J., and Jonassen, M. O., "First Results of Turbulence Measurements in a Wind Park with the Small Unmanned Meteorological Observer SUMO," *Energy Procedia*, Vol. 24, 2012, pp. 176–185. https://doi.org/10.1016/j.egypro.2012.06.099.

[56] Lie, F. A. P., and Gebre-Egziabher, D., "Synthetic Air Data System," *Journal of Aircraft*, Vol. 50, No. 4, 2013, pp. 1234–1249. https://doi.org/10.2514/1.c032177.

[57] Cho, A., Kim, J., Lee, S., and Kee, C., "Wind Estimation and Airspeed Calibration Using a UAV with a Single-Antenna GPS Receiver and Pitot Tube," *IEEE Transactions on Aerospace and Electronic Systems*, Vol. 47, No. 1, 2011, pp. 109–117. https://doi.org/10.1109/taes.2011.5705663.

[58] Johansen, T. A., Cristofaro, A., Sørensen, K., Hansen, J. M., and Fossen, T. I., "On Estimation of Wind Velocity, Angle-of-Attack and Sideslip Angle of Small UAVs Using Standard Sensors," *2015 International Conference on Unmanned Aircraft Systems (ICUAS)*, IEEE Pages 510–519, 2015. https://doi.org/10.1109/icuas.2015.7152330.

[59] Brossard, M., Condomines, J.-P., and Bonnabel, S., "Tightly Coupled Navigation and Wind Estimation for Mini UAVs," *AIAA Guidance, Navigation, and Control Conference*, AIAA Paper 2018-1843, 2018. https://doi.org/10.2514/6.2018-1843.

[60] Cho, A., Kang, Y.-s., Park, B.-j., and Yoo, C.-s., "Airflow Angle and Wind Estimation Using GPS/INS Navigation Data and Airspeed," *2013 13th International Conference on Control, Automation and Systems (ICCAS)*, IEEE Pages 1321–1324, 2013. https://doi.org/10.1109/iccas.2013.6704159.

[61] Wenz, A., Johansen, T. A., and Cristofaro, A., "Combining Model-Free and Model-Based Angle of Attack Estimation for Small Fixed-Wing UAVs Using a Standard Sensor Suite," *International Conference on Unmanned Aircraft Systems*, IEEE Pages 624–632, 2016. https://doi.org/10.1109/icuas.2016.7502583.

[62] Ryu, H., and Park, S., "Vision-Based Wind and Position Estimation with Fixed-Wing Unmanned Aerial Vehicle," *Journal of Guidance, Control, and Dynamics*, Vol. 41, No. 10, 2018, pp. 2283–2292. https://doi.org/10.2514/1.g003646.

[63] Guilliard, I., Rogahn, R., Piavis, J., and Kolobov, A., "Autonomous Thermalling as a Partially Observable Markov Decision Process (Extended Version)," *arXiv preprint arXiv:1805.09875*, 2018.

[64] Rhudy, M. B., Gu, Y., Gross, J. N., and Chao, H., "Onboard Wind Velocity Estimation Comparison for Unmanned Aircraft Systems," *IEEE Transactions on Aerospace and Electronic Systems*, Vol. 53, No. 1, 2017, pp. 55–66. https://doi.org/10.1109/taes.2017.2649218.

[65] Rhudy, M. B., Larrabee, T., Chao, H., Gu, Y., and Napolitano, M., "UAV Attitude, Heading, and Wind Estimation Using GPS/INS and an Air Data System," *AIAA Guidance, Navigation, and Control Conference*, AIAA Paper 2013-5201, 2013. https://doi.org/10.2514/6.2013-5201.

[66] Youn, W., Choi, H. S., Ryu, H., Kim, S., and Rhudy, M. B., "Model-Aided State Estimation of HALE UAV with Synthetic AOA/SSA for Analytical Redundancy," *IEEE Sensors Journal*, Vol. 20, No. 14, 2020, pp. 7929–7940. https://doi.org/10.1109/jsen.2020.2981042.

[67] Rhudy, M. B., Gu, Y., and Chao, H., "Wind Field Velocity and Acceleration Estimation Using a Small UAV," *AIAA Modeling and Simulation Technologies Conference*, AIAA Paper 2014-2647, 2014. https://doi.org/10.2514/6.2014-2647.

[68] Notter, S., Schrapel, P., Groß, P., and Fichter, W., "Estimation of Multiple Thermal Updrafts Using a Particle Filter Approach," *AIAA Guidance, Navigation, and Control Conference*, AIAA Paper 2018-1854, 2018. https://doi.org/10.2514/6.2018-1854.

[69] Mayer, S., Hattenberger, G., Brisset, P., Jonassen, M. O., and Reuder, J., "A 'No-Flow-Sensor' Wind Estimation Algorithm for Unmanned Aerial Systems," *International Journal of Micro Air Vehicles*, Vol. 4, No. 1, 2012, pp. 15–29. https://doi.org/10.1260/1756-8293.4.1.15.

[70] Park, S., "Autonomous Crabbing by Estimating Wind Using Only GPS Velocity," *IEEE Transactions on Aerospace and Electronic Systems*, Vol. 52, No. 3, 2016, pp. 1399–1407. https://doi.org/10.1109/taes.2016.140491.

[71] Hong, H., Wang, M., Holzapfel, F., and Tang, S., "Fast Real-Time Three-Dimensional Wind Estimation for Fixed-Wing Aircraft," *Aerospace Science and Technology*, Vol. 69, 2017, pp. 674–685. https://doi.org/10.1016/j.ast.2017.07.019.

[72] Borup, K. T., Fossen, T. I., and Johansen, T. A., "A Machine Learning Approach for Estimating Air Data Parameters of Small Fixed-Wing UAVs Using Distributed Pressure Sensors," *IEEE Transactions on Aerospace and Electronic Systems*, Vol. 56, No. 3, 2020, pp. 2157–2173. https://doi.org/10.1109/taes.2019.2945383.

[73] Allison, S., Bai, H., and Jayaraman, B., "Wind Estimation Using Quadcopter Motion: A Machine Learning Approach," *Aerospace Science and Technology*, Vol. 98, 2020, p. 105699. https://doi.org/10.1016/j.ast.2020.105699.

[74] Sun, K., Regan, C. D., and Egziabher, D. G., "GNSS/INS Based Estimation of Air Data and Wind Vector Using Flight Maneuvers," *2018 IEEE/ION Position, Location and Navigation Symposium (PLANS)*, 2018, pp. IEEE Pages 838–849. https://doi.org/10.1109/plans.2018.8373461.

[75] Sun, K., Regan, C. D., and Gebre-Egziabher, D., "Observability and Performance Analysis of a Model-Free Synthetic Air Data Estimator," *Journal of Aircraft*, Vol. 56, No. 4, 2019, pp. 1471–1486. https://doi.org/10.2514/1.c035290.

[76] Bishop, G., and Welch, G., "An Introduction to the Kalman Filter," *Proc of SIGGRAPH, Course*, Vol. 8, No. 27599-23175, 2001, p. 41.

[77] PX4, "Using the ECL EKF," , 2020. URL https://docs.px4.io/v1.9.0/en/advanced_config/tuning_the_ecl_ekf.html.

[78] Chao, H., Gu, Y., Tian, P., Zheng, Z. C., and Napolitano, M. R., "Wake Vortex Detection with UAV Close Formation Flight," *AIAA Atmospheric Flight Mechanics Conference*, AIAA Paper 2015-2396, 2015. https://doi.org/10.2514/6.2015-2396.

[79] Jategaonkar, R., *Flight Vehicle System Identification: A Time Domain Methodology*, Vol. 216, AIAA Progress in Astronautics and Aeronautics, AIAA, Reston, VA, 2006. https://doi.org/10.2514/4.866852.

[80] Rodriguez, L., Cobano, J. A., and Ollero, A., "Wind Field Estimation and Identification Having Shear Wind and Discrete Gusts Features with a Small UAS," *2016 IEEE/RSJ International Conference on Intelligent Robots and Systems (IROS)*, IEEE Pages 5638–5644, 2016. https://doi.org/10.1109/iros.2016.7759829.

[81] Langelaan, J. W., Spletzer, J., Montella, C., and Grenestedt, J., "Wind Field Estimation for Autonomous Dynamic Soaring," *2012 IEEE International Conference on Robotics and Automation*, IEEE Pages 16–22, 2012. https://doi.org/10.1109/icra.2012.6224954.

[82] Tian, P., Chao, H., and Wu, H., "UAS-based Wind Estimation Using Sinusoidal Gust Model," *AIAA Atmospheric Flight Mechanics Conference*, AIAA Paper 2019-1597, 2019. https://doi.org/10.2514/6.2019-1597.

[83] Cornman, L. B., *Airborne In Situ Measurements of Turbulence*, Springer International Publishing, 2016. https://doi.org/10.1007/978-3-319-23630-8_5.